Organic & Biomolecular Chemistry

PAPER

View Article Online
View Journal | View Issue

Check for updates

Cite this: *Org. Biomol. Chem.*, 2025, **23**, 10174

Diastereoselective amidoboronate formation and transformation from a *rac* to a different *meso* amidoboronate *via* dynamic C–C bonds

Patrick Harders,[a,b] Tim Raeker,[c] Lorenz Pietsch,[a] Christian Näther,[d] Bernd Hartke[c] and Anna J. McConnell *[a,b]

Amidoboronates, synthesized through the reductive coupling of iminoboronates with cobaltocene in DMSO, form as mixtures of up to three isomers (rac_5, rac_6 and $meso_5$) and can exhibit up to three types of dynamic covalent bonds (C–C, B–N, B–O). In order to exploit the reductive coupling for the self-assembly of covalent organic macrocycles and cages, control over the diastereoselectivity and reversibility of C–C bond formation is required. We report proof-of-principle in dimeric amidoboronates; diastereoselective *rac* isomer formation was observed for amidoboronate **5e** (based on *p*-NMe_2-substituted aniline, pyrocatechol and phenylboronate), whereas employing an iminoboronate containing *p*-OMe-substituted aniline, either pyro- or tetrachlorocatechol and 3-fluorophenylboronate led to rare examples of *meso* diastereoselectivity (9 : 1 dr for **7d** and **8d**). The addition of a second iminoboronate to amidoboronate reaction mixtures probed the reversibility of C–C bond formation as evidenced by the formation of new homo- and cross-coupled amidoboronates *via* exchange. The dynamic covalent C–C bonds were exploited in the unprecedented diastereoselective transformation of ***rac*$_{5/6}$-5e** to ***meso*$_5$-7d** following addition of excess iminoboronate **3d**.

Received 15th September 2025,
Accepted 14th October 2025

DOI: 10.1039/d5ob01479d

rsc.li/obc

Open Access Article. Published on 16 October 2025. Downloaded on 12/25/2025 7:24:13 PM.
This article is licensed under a Creative Commons Attribution 3.0 Unported Licence.

Introduction

Dynamic covalent chemistry[1–7] exploits reversible bond formation for applications from the self-assembly of macrocycles[8–13] and cages[14,15] to self-healing polymers.[16–18] Reversible C–C bond formation involving a radical/dimer equilibrium has emerged as a new tool in dynamic covalent chemistry, requiring a low bond dissociation energy for the dimer and stabilization of the radical, *e.g.* through spin delocalization.[4] While carbon-based radicals including dicyanomethyl derivatives[4,10,19–23] have been employed to self-assemble macrocycles,[10–13] radical-based dynamic covalent chemistry is still relatively underdeveloped. Furthermore, the discovery of new types of dynamic covalent bonds would expand the dynamic covalent chemistry toolbox and could enable the design of more complex systems with multiple orthogonal dynamic covalent bonds.[5]

We recently reported the reductive coupling of *N*-aryl iminoboronates gives up to three amidoboronate products with interesting dynamic covalent chemistry:[24–26] diastereomeric 5-membered rac_5 and $meso_5$ isomers as well as a unique 6-membered rac_6 isomer formed from interconversion of the rac_5 isomer *via* dynamic covalent BN bonds. While the *rac* and $meso_5$ isomers have not been observed to interconvert upon heating solutions of redissolved crystals,[24,26] the rac_5/rac_6 ratio could be tuned by exploiting not only dynamic covalent BN bonds but also BO bonds by exchanging pyrocatechol for tetrachlorocatechol.[25]

Based on the angles between the *p*-aniline substituents in amidoboronate X-ray crystal structures varying from approx. 65° ($meso_5$ for conformation with *gauche* protons) to 90° (rac_5) and 120° (rac_6),[24–26] we envisaged the reductive coupling could be exploited for the self-assembly of covalent organic macrocycles and cages. However, this necessitates that C–C bond formation occurs: (a) reversibly so that the reductive coupling proceeds under thermodynamic control; (b) diastereoselectively so that the connectivity between building blocks either has a *meso* or *rac* configuration.

For related reductive couplings such as the pinacol coupling,[27–30] *rac* diastereoselectivity has been observed with

[a]*Otto Diels Institute of Organic Chemistry, Christian-Albrechts-Universität zu Kiel, Otto-Hahn-Platz 4, Kiel D-24098, Germany*
[b]*Department of Chemistry and Biology, University of Siegen, Adolf-Reichwein-Strasse 2, Siegen D-57076, Germany. E-mail: anna.mcconnell@uni-siegen.de*
[c]*Institute of Physical Chemistry, Christian-Albrechts-Universität zu Kiel, Max-Eyth-Strasse 2, Kiel D-24118, Germany*
[d]*Institute of Inorganic Chemistry, Christian-Albrechts-Universität zu Kiel, Max-Eyth-Strasse 2, Kiel D-24118, Germany*

This journal is © The Royal Society of Chemistry 2025

Open Access Article. Published on 16 October 2025. Downloaded on 12/25/2025 7:24:13 PM.
This article is licensed under a Creative Commons Attribution 3.0 Unported Licence.

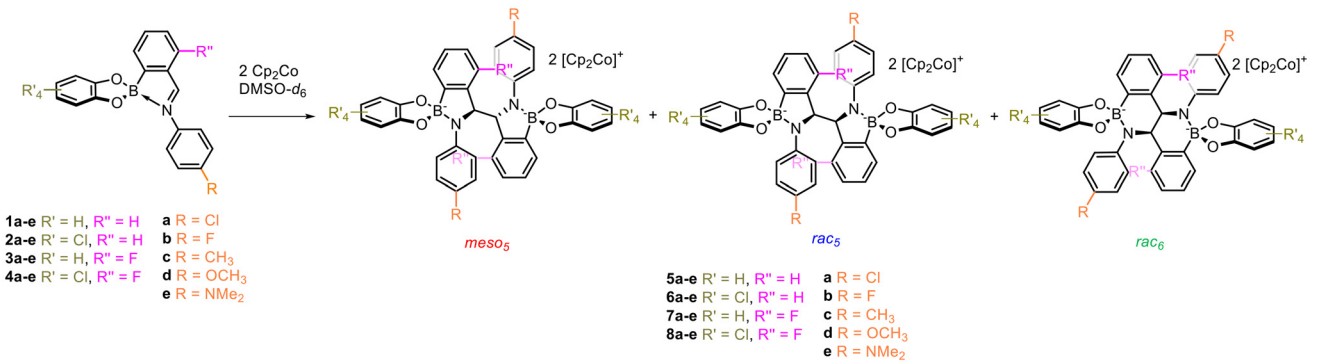

Scheme 1 Reductive coupling of iminoboronates **1a–e**, **2a–e**, **3a–e** and **4a–e** to the corresponding amidoboronates.

several metal-based reductants where the metal is proposed to either bridge[31–35] or preorganize[36,37] the coupling partners. In some reductive couplings, the *rac*/*meso* ratio has also been observed to change over time, attributed to reversible C–C bond formation *via* a radical/dimer equilibrium[38] rather than epimerization.[39] However, there are fewer examples of *meso* diastereoselective reductive couplings.[40–42]

Reductive couplings giving access to BN-containing heterocycles[43,44] have been less well-studied and often report the formation of diastereomeric mixtures.[45,46] However, Dostál and co-workers reported heating converted the *meso* to the *rac* isomer.[45] Furthermore, subsequent reduction of the dimer yielded the BN analogue of the indenyl anion and reaction of this with the iminochloroborane was implicated as a second pathway to dimer formation.

These literature precedents demonstrate the promise for exploiting the reductive coupling in the self-assembly of amidoboronate-based macrocycles and cages. However, given that complex mixtures could be obtained considering the three possible types of connectivity between the building blocks (*e.g.* $meso_5$, rac_5 and rac_6), we focused on dimeric amidoboronates as model systems to understand how varying the electronic properties of the aniline, catechol and boronic acid subcomponents (Scheme 1) influences the diastereoselectivity and reversibility of C–C bond formation. We report not only access to the *rac* and *meso* isomers in high diastereoselectivity but also demonstrate the ability for some amidoboronates to undergo C–C bond exchange reactions upon the addition of a second iminoboronate. Finally, we exploited knowledge of the diastereoselectivity and reversible C–C bond formation in a diastereoselective transformation from a *rac* isomer to a different *meso* diastereomer, demonstrating proof-of-principle for the use of the reductive coupling in self-assembly applications.

Results and discussion

Previously, we demonstrated that the reductive coupling of iminoboronates **1a–e** and **2a–e** in acetonitrile gave different mixtures of ***meso*$_5$-5/6**, ***rac*$_5$-5/6** and ***rac*$_6$-5/6** where each amidoboronate isomer has a characteristic methine signal between 4 and 6 ppm in the ^{1}H NMR spectra (Scheme 1).[24–26] However, there are limits to characterization since: (i) radical species are likely to be NMR silent or difficult to characterize due to their paramagnetic nature; (ii) crystallization of one amidoboronate product from the acetonitrile reaction mixture prevented determination of the product distribution.

Here, analogous reductive couplings of iminoboronates **1–4** using cobaltocene as the reductant were carried out in DMSO-d_6 to investigate the influence of the *para*-aniline (orange R, Scheme 1), catechol (dark yellow R′) and phenylboronate (magenta R″) substituents on the product distribution since competing crystallization could be prevented. The relative ratio of the amidoboronate species was investigated rather than their quantitative yield since radical species could not be quantified and the formation of other products could not be excluded due to complex ^{1}H NMR spectra where signal overlap in the comparatively small chemical shift range complicated NMR analysis.

Furthermore, a fluorine tag was introduced into iminoboronate motifs **3a–e** and **4a–e** to simplify reaction mixture analysis by taking advantage of the wider chemical shift range of ^{19}F NMR spectroscopy as well as the higher responsiveness to chemical environment changes.[47] The 3-position of the boronic acid subcomponent was chosen since 3-fluoro-2-formylphenylboronic acid is commercially available and substitution of the boronic acid subcomponent has not been investigated in previous reductive couplings.[24–26]

Iminoboronates **1a–e** and **2a–e** were synthesized as previously reported[24,25] from the respective *p*-substituted aniline, catechol and 2-formylphenylboronic acid subcomponents. Related iminoboronates **3a–e** and **4a–e** employing the ^{19}F phenylboronate tag were prepared similarly from 3-fluoro-2-formylphenylboronic acid (SI sections 2.2–2.5 and 2.7–2.10), although it was necessary to use an alternative isolation procedure for iminoboronates **3e** and **4e** (SI sections 2.6 and 2.11). X-ray crystal structures of **3a** and **4d** were similar to those previously reported for **1a**,[25] **1d**,[25] **1e**[25] and **2d**[25] showing a tetrahedral boron center and B–N dative bond (SI sections 2.2.1 and 2.10.1).

Open Access Article. Published on 16 October 2025. Downloaded on 12/25/2025 7:24:13 PM.
This article is licensed under a Creative Commons Attribution 3.0 Unported Licence.

The reductive couplings of all iminoboronates were carried out in DMSO-d_6 in a glovebox under a nitrogen atmosphere in J. Young NMR tubes using 1.0–1.2 equivalents of cobaltocene as the reductant to ensure full conversion to the amidoboronate dimers. ^{1}H NMR spectra and, where applicable, ^{19}F NMR spectra were recorded over time. Given the formation of multiple products, the reaction mixtures were characterized as thoroughly as possible (SI, section 3), including comparison to previously reported solution structures of single isomers determined from redissolved crystals.[24,25] For the amidoboronates with a ^{19}F tag, ^{19}F signal assignment to a particular isomer *via* integration and correlation to the corresponding ^{1}H NMR methine integrals was difficult due to the broadness of some ^{19}F signals. This and overlapping signals with side-products prevented the use of ^{19}F spectroscopy for determining the product distributions. However, the *meso*$_5$, *rac*$_5$ and *rac*$_6$ isomers themselves were tentatively assigned by comparison of the ^{19}F spectra within a series (SI sections 4.3.2 and 4.4.2).

The relative *meso*$_5$/*rac*$_5$/*rac*$_6$ isomeric ratio following equilibration of the reaction mixtures for at least 72 hours was determined by integrating and normalizing the characteristic ^{1}H NMR methine singlet[24–26] for each amidoboronate isomer (Fig. 1, SI section 4). The diastereoselectivity of a reductive coupling is determined by the *meso*$_5$/*rac* ratio where *rac* is the sum of the *rac*$_5$ and *rac*$_6$ isomers since the *rac*$_5$/*rac*$_6$ interconversion does not involve C–C bond formation but rather rearrangement of the B–N bonds.[24–26] Beyond the methine singlets for the three expected amidoboronate isomers, two broad signals appeared in the same region in many reductive couplings (Fig. S181). These signals are attributed to a cobaltocene derivative formed from the addition of an amidoboronate (see below and SI section 6 for identification of this derivative). This cobaltocene derivative was not included in the isomer quantification.

For the reductive couplings of pyrocatechol-based iminoboronates **1a–d**, a near statistical mixture of the *meso* and *rac*$_{5/6}$ products was observed (Fig. 1a, SI section 4.1). Interestingly, the reductive coupling of **1e** with the most electron-rich aniline substituent NMe_2 was diastereoselective as only the ***rac*$_5$-5e** and the ***rac*$_6$-5e** products were observed. For

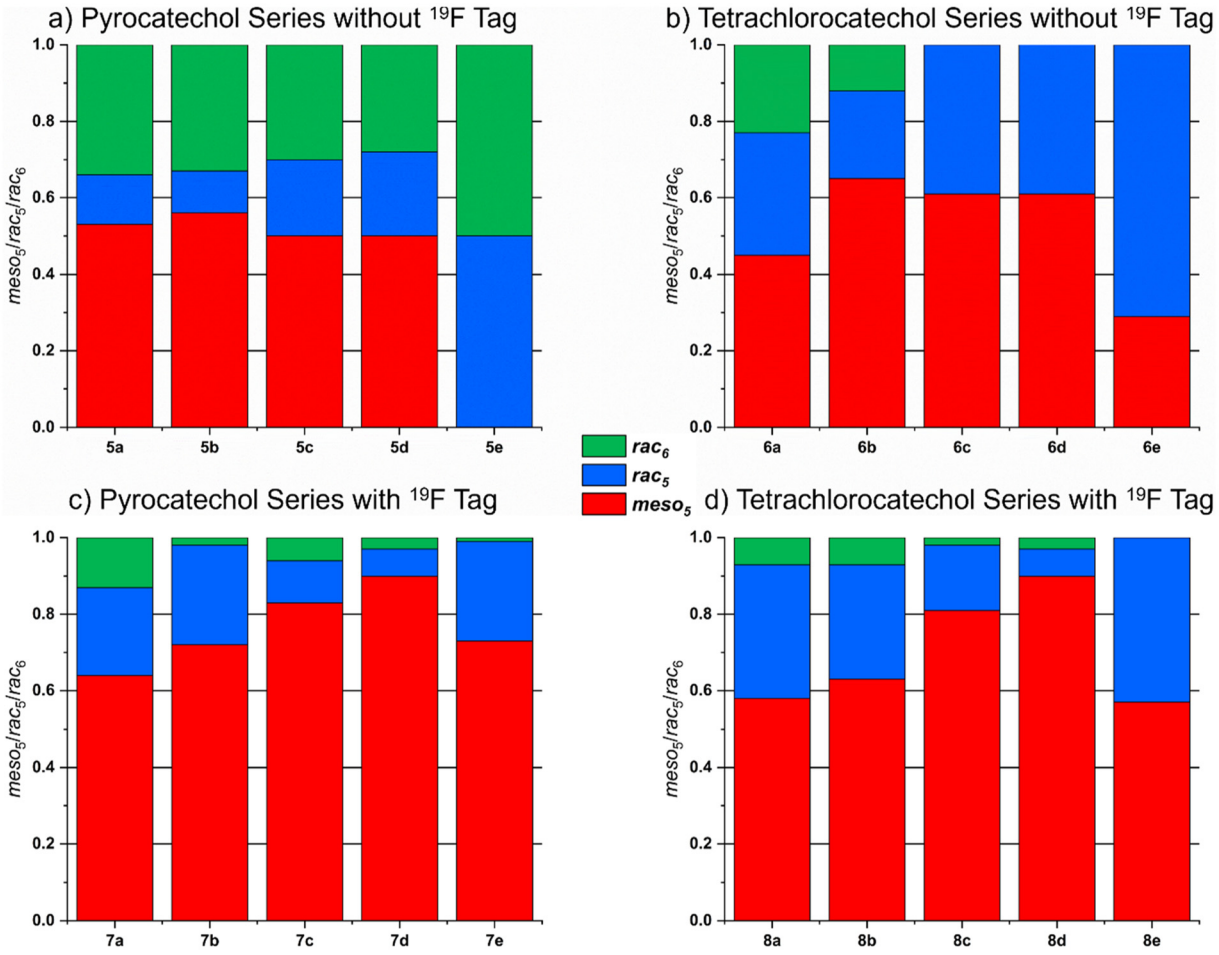

Fig. 1 Product distribution following the reductive coupling to: (a) pyrocatechol-based amidoboronates **5a–e** without a ^{19}F phenylboronate tag; (b) tetrachlorocatechol-based amidoboronates **6a–e** without a ^{19}F phenylboronate tag; (c) pyrocatechol-based amidoboronates **7a–e** with a ^{19}F phenylboronate tag; (d) tetrachlorocatechol-based amidoboronates **8a–e** with a ^{19}F phenylboronate tag. *p*-Aniline substituents: **a** Cl; **b** F; **c** CH_3; **d** OMe; **e** NMe_2.

This journal is © The Royal Society of Chemistry 2025

Open Access Article. Published on 16 October 2025. Downloaded on 12/25/2025 7:24:13 PM. This article is licensed under a Creative Commons Attribution 3.0 Unported Licence.

the tetrachlorocatechol series (**6a–e**), all three products were observed for **6a** and **6b**, whereas only the *meso*$_5$ and *rac*$_5$ isomers were observed for amidoboronates **6c–e** (Fig. 1b, SI section 4.2). For **6b–d**, the *meso*$_5$ isomer was the main product, whereas the major isomer for **6e** was *rac*$_5$.

Interestingly, the introduction of ^{19}F phenylboronate tags onto amidoboronates **7a–e** and **8a–e** changed the product distributions compared to amidoboronates **5a–e** and **6a–e** (Fig. 1c, d, SI sections 4.3–4.4); the three isomers formed in every reductive coupling (with the exception of **8e**), contrasting **6c** and **6d** where the *rac*$_6$ species was not observed. The amount of the *rac*$_6$ species for **7a–d** and **8a–b** was reduced compared to the analogous reductive coupling **5a–d** and **6a–b**. Furthermore, the *meso*$_5$ isomer predominated in the amidoboronate mixtures with the ^{19}F phenylboronate tag and the *meso*$_5$ fraction increased from approximately 60% to 90% as the electron-donating ability of the *p*-aniline substituent increased from Cl (**7a** and **8a**) to OMe (**7d** and **8d**). However, for **7e** and **8e** with *p*-NMe$_2$ aniline substituents, the amount of the *meso*$_5$ isomer decreased relative to **7d** and **8d**, respectively.

Comparing the series of reductive couplings, several trends emerged. Amidoboronates **5a–5d**, **7a–7e** and **8a–8d** with Cl to OMe/NMe$_2$ aniline substituents formed as a mixture of all three isomers (*meso*$_5$, *rac*$_5$, *rac*$_6$), as did tetrachlorocatechol-based amidoboronates **6a/b** with electron-withdrawing Cl and F substituents. In contrast, only two isomers, *meso*$_5$ and *rac*$_5$, were observed for **6c–6e** as well as **8e**. Interestingly, three reductive couplings were highly diastereoselective; the reductive coupling to **5e** was diastereoselective for the *rac* isomer only (forming as a 1 : 1 mixture of the *rac*$_5$ and *rac*$_6$ isomers), whereas the *meso*$_5$ isomer was obtained in a 9 : 1 diastereomeric ratio (dr) for **7d** and **8d** with *p*-OMe aniline substituents and a ^{19}F-tagged phenylboronate. However, amidoboronates **7e** and **8e** with NMe$_2$ substituents did not appear to follow the trend of increasing diastereoselectivity for *meso*$_5$ with increasing electron-donating ability of the *p*-aniline substituent. Similarly, the product distributions for **5e** and **6e** differed from those within the corresponding series with the *rac* isomer as the only or predominant product, respectively. Thus, we propose *p*-NMe$_2$ substituents may have a *rac*-directing effect and/or C–C bond formation may be reversible.

To rationalize why the *meso*$_5$ isomer forms preferentially with the ^{19}F-tagged amidoboronates **7** and **8**, analogous reductive couplings were carried out in acetonitrile in an effort to obtain single crystals. While a single amidoboronate isomer typically crystallized from previously reported reductive couplings in acetonitrile,[24–26] crystals were only obtained from the reductive coupling of **4d**. Surprisingly, the X-ray structure reveals an unusual nine-membered ring system, where the two boron centers are bridged by an oxygen atom and no longer bonding to nitrogen, thus breaking the bicyclic amidoboronate structure (Fig. 2, SI section 3.4.4.1). However, the C–C bond has a *meso* configuration consistent with observation of the *meso*$_5$ isomer as the major product from the reductive coupling. We propose this nine-membered ring system is a water adduct of **8d** where traces of water add to the two B–N covalent

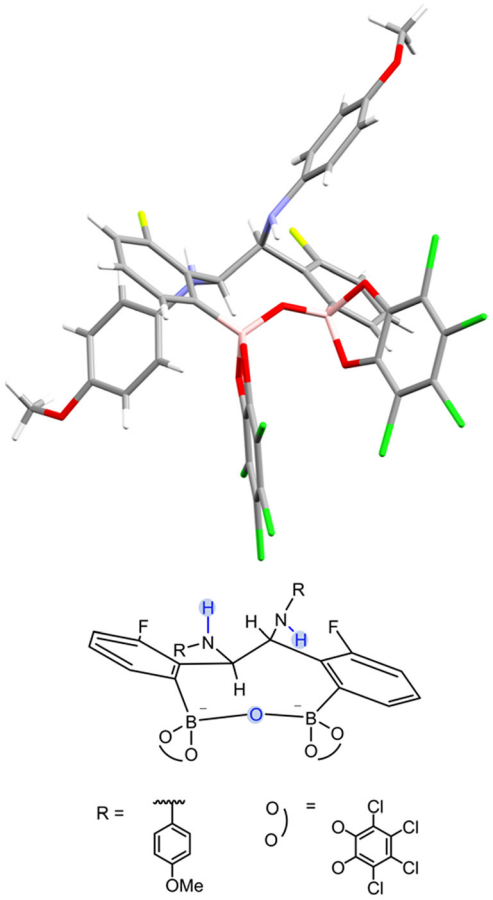

Fig. 2 Crystal structure of the water adduct of **8d** with the structure below depicting the nine-membered ring with the atoms proposed to originate from the addition of water shown in blue. For clarity, the Cp_2Co^+ countercations and solvent molecules have not been depicted.

bonds in a similar fashion to the addition of water/solvent across B–N dative bonds in related *o*-aminomethylphenylboronate esters[48–51] and subsequent elimination of a molecule of water forms the unique heterocyclic ring system. Unfortunately, difficulties reproducing the crystallization of this adduct prevented further studies, *e.g.* redissolving the crystals to determine the solution structure.

Intrigued by the observed diastereoselectivity for ***rac*$_{5/6}$-5e** and ***meso*$_5$-7d/8d** and the change in product distributions for the reductive couplings as a function of the aniline, catechol and phenylboronate substituents, we investigated whether the reductive couplings proceed under kinetic or thermodynamic control; irreversible C–C bond formation under kinetic control would result in a product distribution determined by the relative transition state energies of the *rac*$_5$ and *meso*$_5$ isomers, whereas reversible C–C bond formation (*e.g.* through a radical/dimer equilibrium) would give a product distribution reflecting the relative thermodynamic stability of the isomers and give the necessary error-checking needed for use of the reductive coupling in self-assembly applications.

Open Access Article. Published on 16 October 2025. Downloaded on 12/25/2025 7:24:13 PM.
This article is licensed under a Creative Commons Attribution 3.0 Unported Licence.

In related dicyanomethyl radical systems, several groups have reported electron-donating substituents *para* to the radical led to dynamic covalent C–C bonds due to stabilization of the radical by spin delocalization,[10,19–23,52,53] attributed to the captodative effect.[22,54,55] Winter and co-workers reported the Hammett parameter of the *para*-substituent correlated with the dimerization binding constant,[21] while Sakamaki, Seki and co-workers found the spin density on the central dicyanomethyl carbon correlated with the bond dissociation energy.[19] In cases of an equilibrium between the radical and dimer, a lengthening of the C–C bond to 1.63–1.65 Å was also observed in X-ray crystal structures.[19]

Given the product distributions for the NMe_2-substituted amidoboronates **5–8e** did not follow the trends observed for the Cl- to OMe-substituted amidoboronates within the same series, we hypothesized spin density delocalization due to the electron-donating nature of the NMe_2 substituents as well as electron delocalization over the catechol subcomponent could stabilize the radical sufficiently to allow reversible C–C bond formation. However, the C–C amidoboronate bond length in the X-ray crystal structure of ***rac*$_5$-6e** was similar to those for other amidoboronates (*e.g.* **5a–d**, **6a**, **6c–d**) and consistent with a C–C single bond.[24–26] Furthermore, our spin density calculations did not show a significant difference for different *p*-aniline substituted amidoboronates since the spin was largely localized on the imine carbon (SI section 5.1). These X-ray and computational results suggest that the dimer is favored over the radical form.

Instead, we hypothesized that the radical could be stabilized and amidoboronate dimer formation could be hindered by introducing sterically bulky *o*-Me groups on the aniline.[39] Hence, iminoboronate **2f** based on 2,4,6-trimethylaniline was prepared (SI section 2.1) and the reductive coupling with cobaltocene was carried out (Scheme 2, SI section 6.1.1).

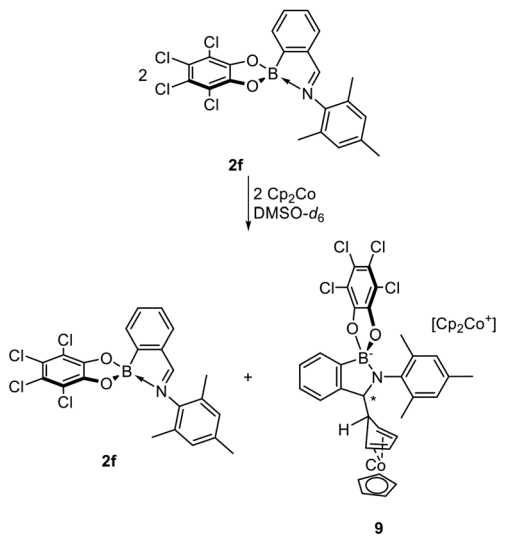

Scheme 2 Reductive coupling of sterically bulky iminoboronate **2f** leading to a 1 : 1 mixture of unreacted iminoboronate **2f** and a cobaltocene derivative proposed to be *exo*-functionalised **9**.

Surprisingly, a different product formed as a 1 : 1 mixture with unreacted iminoboronate **2f**; the NMR signals of this diamagnetic product were consistent with the species with two broad signals in the methine region previously observed in some reaction mixtures (Fig. S181). NMR analysis revealed: (i) a significantly upfield shifted amidoboronate methine (now a doublet) at 2.92 ppm; (ii) a singlet around 4.6 ppm corresponding to a cyclopentadienyl ring; (iii) a ring system with five signals from 2–3 ppm including a dt coupling to the amidoboronate methine, suggesting a η^4-coordinated cyclopentadiene (Fig. S183). Thus, we propose **9** as the structure of this cobaltocene derivative based on the similarity of the NMR spectrum to related cobaltocene additionproducts.[56–61] However, unlike the AA′XX′ spin systems observed for these compounds, the cyclopentadiene signals in **9** are diastereotopic due to the presence of the stereogenic centre (* in Scheme 2). Furthermore, desymmetrization of the aniline proton signals of **9** suggests hindered rotation around the aniline C–N bond. Due to steric hindrance, **9** is also most likely the *exo* isomer with the chemical shift of 2.76 ppm consistent with an *endo* H.[58,59]

Further characterization of **9** by X-ray crystallography and mass spectrometry was attempted through analogous reductive couplings in acetonitrile (SI section 6.1.2). Full conversion to the cobaltocene addition product was observed by NMR spectroscopy employing two equivalents of cobaltocene, suggesting two-electron reduction is involved (Fig. S188). However, mass spectrometric analysis of this reaction mixture revealed a signal at *m*/*z* 496, which is lower than expected for **9** (Fig. S189). Instead, this is attributed to a decomposition product of **9**, where the carbon–carbon bond to the cyclopentadiene ring is broken and water adds across the B–N bond. Additionally, the ESI mass spectrum in positive mode shows only the presence of Cp_2Co^+ (Fig. S190).

Disappointingly, numerous attempts to crystallize **9** or related cobaltocene addition products from analogous reductive couplings in acetonitrile were unsuccessful. Therefore, the geometry for the proposed structure of **9** was optimized in calculations and conformational analysis was performed to investigate how steric hindrance could account for the desymmetrized aniline signals compared to analogues without *o*-aniline substituents (SI section 6.1.3). Furthermore, NMR and ESI mass spectra from previously reported reductive couplings[25] were re-analysed and these provided further evidence for the formation of cobaltocene addition products as another product from the reductive coupling (SI section 6.2).

Cobaltocene addition products have been proposed to form from radical addition to Cp_2Co[59] or nucleophilic addition to Cp_2Co^+.[59,60] Similarly, nucleophilic addition has been implicated as an alternative pathway to radical recombination in dimer formation from the related reductive coupling by Dostál and coworkers where two-electron reduction of the iminochloroborane to the BN-analogue of the indenyl anion and subsequent addition to a second iminochloroborane gave dimers.[45] Furthermore, reductive C–C bond cleavage of the dimer by two equivalents of reductant gave the BN-analogue of the indenyl anion.

This journal is © The Royal Society of Chemistry 2025

Open Access Article. Published on 16 October 2025. Downloaded on 12/25/2025 7:24:13 PM.
This article is licensed under a Creative Commons Attribution 3.0 Unported Licence.

To investigate whether two-electron reduction could play a role in the reductive coupling of iminoboronates, control reductive couplings of **1b** and **1e** were carried out with an excess of cobaltocene (5 equivalents); for the reductive coupling of **1b** (SI section 6.3.1), the amount of the cobaltocene addition product significantly increased relative to amidoboronate products with excess *vs.* 1 equivalent of cobaltocene, suggesting the formation of the cobaltocene addition product *via* two-electron reduction is feasible and outcompetes amidoboronate dimer formation and/or reductive C–C cleavage of the dimer to the cobaltocene addition product occurs with excess reductant (Fig. S198).

In contrast, no cobaltocene addition product was observed for the reductive coupling of **1e** with excess reductant (SI section 6.3.2). Instead, a third set of signals with a methine signal consistent with ***meso*$_5$-5e** were observed at short reaction times and this set of signals diminished and largely disappeared over time (Fig. S199). This suggests that the reductive coupling of **1e** is under thermodynamic control since the formation of the *meso* isomer is reversible and this could account for the observed diastereoselectivity for the *rac* isomers.

Therefore, the reversibility of C–C bond formation was probed across the series of amidoboronates through exchange reactions where a second iminoboronate (purple square, Fig. 3a) was added to amidoboronate product mixtures (orange dimers); in cases where C–C bond formation is reversible (*e.g. via* a radical/dimer equilibrium or oxidative decoupling), the formation of cross-coupled amidoboronate products (orange and purple dimer) or potentially homo-coupled dimers of the added iminoboronate (purple dimer) would be expected along with liberation of the iminoboronate (orange square) following exchange. ^{1}H NMR spectra were recorded over time and analyzed for signals of the released orange iminoboronate, as well as new signals in the methine, methoxy and methyl regions, where applicable (SI sections 5.2–5.5).

For all series, the *p*-F-aniline substituted iminoboronates (**1–4b**) were added to the amidoboronate reaction mixtures of the same series (to avoid catechol exchange)[25] so that product mixture changes could be additionally monitored by ^{19}F spectroscopy since the ^{19}F signals of the iminoboronates and amidoboronates are in distinct chemical shift ranges. For the *p*-F substituted amidoboronates (**5–8b**), two exchange reactions were carried out, adding either an iminoboronate with an electron-donating *p*-aniline NMe_2 substituent (**1–4e**) or electron-withdrawing *p*-Cl substituent (**1–4a**).

Initially, the electronic effect of the *p*-aniline substituent was investigated within the pyrocatechol series through the exchange reactions of amidoboronates **5a/c–e** with the addition of iminoboronate **1b**. For **5a** with electron-withdrawing *p*-Cl substituents, the ^{1}H NMR spectrum remained largely unchanged with a small decrease of the ***meso*$_5$-5a** signal as well as the appearance of iminoboronate **1a** from exchange (Fig. S114). In the ^{19}F spectra, the major signal is the added **1b** iminoboronate, however, there are other minor signals in the amidoboronate chemical shift range between −128 to −134 ppm (Fig. S115).

In contrast, more significant NMR spectral changes were observed as the electron-donating character of the *p*-aniline substituent increased. For the reactions of **5c** and **5d**, there are new signals in the ^{1}H and ^{19}F NMR spectra that are attributed to the respective cross-coupled products as well as the homo-coupled product **5b** (Fig. S116–S119). For the reaction mixture with *p*-NMe_2 substituents (Fig. 4a–b and S120), the ***rac*$_5$-5e** (blue) and ***rac*$_6$-5e** (green) signals disappeared, signals for lib-

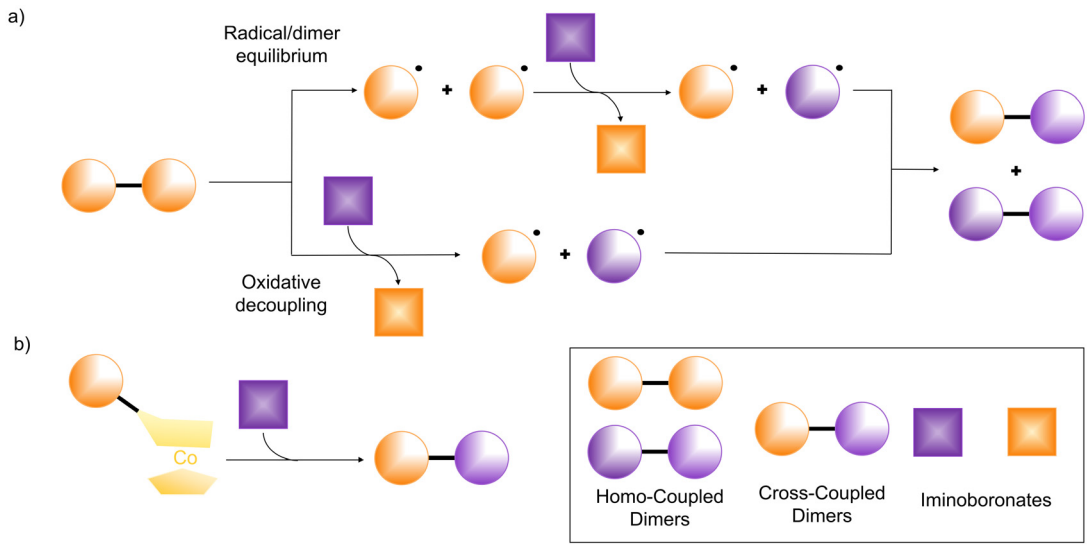

Fig. 3 Exchange reactions probing the reversibility of C–C bond formation in reaction mixtures containing amidoboronate dimers (orange dimer in a) and in some cases, the cobaltocene addition product (in b): addition of a second iminoboronate (purple square) could lead to the formation of cross-coupled dimers (purple and orange dimer) and/or homo-coupled dimers of the added iminoboronate (purple dimer) along with liberation of an iminoboronate (orange square) in the case of (a). Two possible exchange pathways for the orange homo-coupled dimer *via* a radical/dimer equilibrium or oxidative decoupling are depicted in (a) and for simplicity, only radical species are depicted.

Open Access Article. Published on 16 October 2025. Downloaded on 12/25/2025 7:24:13 PM.
This article is licensed under a Creative Commons Attribution 3.0 Unported Licence.

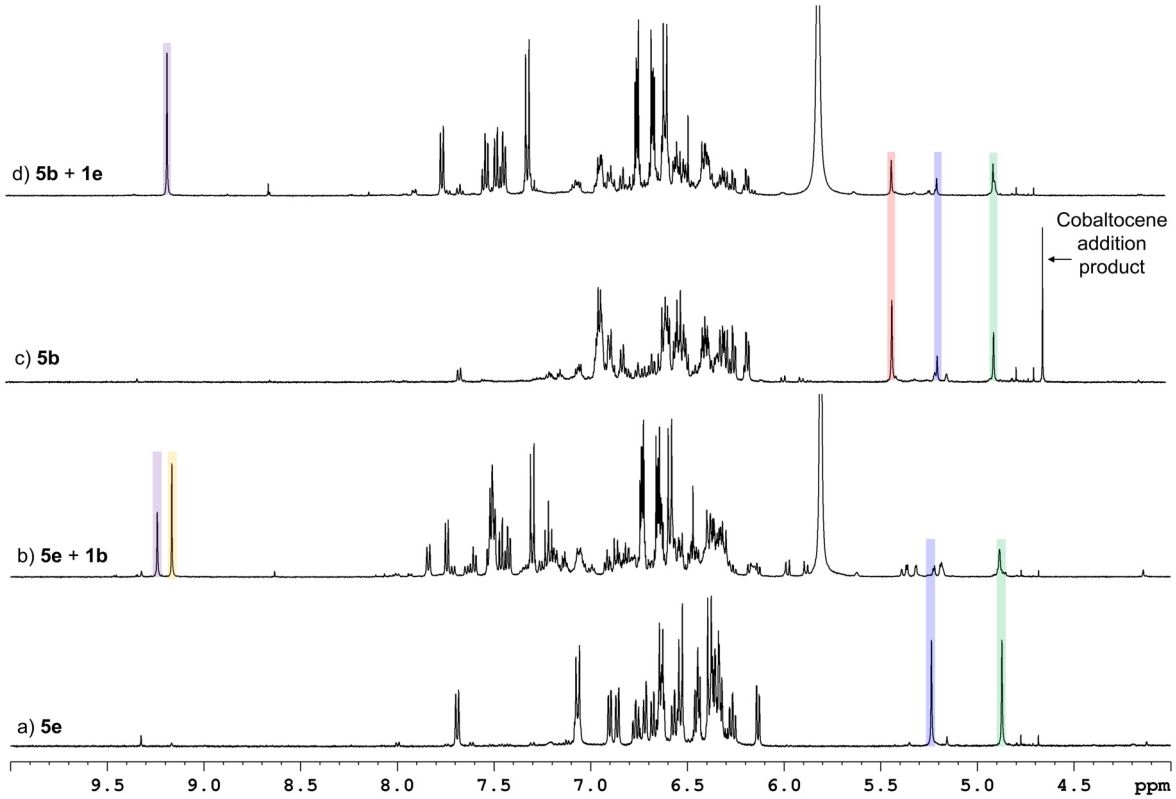

Fig. 4 NMR spectra (500 MHz, DMSO-d_6) of: (a) the reaction mixture **5e** showing a 1 : 1 mixture of ***rac*$_5$-5e** (blue) and ***rac*$_6$-5e** (green); (b) the exchange reaction of **5e** after iminoboronate **1b** (purple) addition showing exchange by desymmetrization of the methine region and release of iminoboronate **1e** (orange); (c) the reaction mixture **5b** showing the presence of ***meso*$_5$-5b** (red), ***rac*$_5$-5b** (blue), ***rac*$_6$-5b** (green) and the cobaltocene addition product; (d) the exchange reaction of **5b** after iminoboronate **1e** (purple) addition showing the loss of the cobaltocene addition product and no iminoboronate **1b** release.

erated iminoboronate **1e** (orange) grew in and the appearance of new signals in the methine region suggested the formation of cross-coupled dimers due to desymmetrization. This is supported by new ^{19}F signals between −110 ppm and −135 ppm that do not correspond to **1b** or its homo-coupled products **5b** (Fig. S121).

The exchange reaction of *p*-F substituted **5b** with iminoboronate **1e** (with an electron-donating *p*-NMe_2 substituent) led to new minor signals in the ^{1}H (Fig. 4c–d and S124) and ^{19}F spectra (Fig. S125); the ^{19}F signals were consistent with those attributed to a cross-coupled dimer formed in the exchange reaction of **5e** with **1b**. However, the release of iminoboronate **1b** was not observed and instead the cobaltocene addition product in the original reaction mixture disappeared (Fig. 4c–d and S124–S125). This suggests that cross-coupled dimer formation does not occur through an exchange reaction of **5b** with **1e**, but rather *via* an alternative pathway where the iminoboronate reacts with the two-electron-reduced cobaltocene addition product (Fig. 3b), as observed for Dostál's related system.[45]

Conversely, different spectral changes were observed upon the addition of **1a** (with an electron-withdrawing *p*-Cl substituent) to **5b**. While all three **5b** isomer signals were still present, a significant reduction of the *meso*$_5$ signals was accompanied by the appearance of iminoboronate **1b** peaks and new methine signals (Fig. S122 and S123). The chemical shifts of these along with the minor changes in the ^{19}F spectrum suggest the formation of homo-coupled amidoboronate **5a** rather than a cross-coupled product.

A number of trends emerged from comparison of the exchange reactions of **5a–e** to the other amidoboronate series **6a–e** (SI section 5.3), **7a–e** (SI section 5.4) and **8a–e** (SI section 5.5). Firstly, the amount of exchange was typically observed to correlate with the increase in the electron-donating ability of the *p*-aniline substituent (from Cl to NMe_2) upon addition of iminoboronates **1–4b**, as exemplified in ^{19}F NMR spectra by the increased ^{19}F incorporation as exchange reaction products (*e.g.* homo- and cross-coupled dimers) relative to the added iminoboronate (Fig. S126 and S140) or increase in liberated iminoboronate relative to added iminoboronate for amidoboronates with a ^{19}F phenylboronate tag (Fig. S157 and S174). In the ^{1}H NMR spectra, the increasing amount of liberated iminoboronate (orange in Fig. 3a) was accompanied by the appearance of new methine signals attributed to cross-coupled/homodimers and/or other exchange reaction products. Additionally, for pyrocatechol and tetrachlorocatechol amidoboronates without a ^{19}F phenylboronate tag, the *meso*$_5$ signals decreased more than the *rac* signals, suggesting that the C–C bond for

 This journal is © The Royal Society of Chemistry 2025

Open Access Article. Published on 16 October 2025. Downloaded on 12/25/2025 7:24:13 PM. This article is licensed under a Creative Commons Attribution 3.0 Unported Licence.

the *meso*$_5$ isomer is the weakest of the three isomers (Fig. S116, S127 and S136).

However, the choice of iminoboronate added also influences the amount of exchange as observed for *p*-F amidoboronates; little to no exchange was observed upon addition of iminoboronates with electron-donating *p*-aniline substituents (NMe_2 or OMe, SI sections 5.2.6, 5.3.6, 5.4.6, 5.4.7, 5.5.6 and 5.5.7), whereas the exchange increased with iminoboronates containing the more electron-withdrawing *p*-Cl aniline substituent as evidenced by the signals corresponding to the released *p*-F iminoboronates (**1–4b**, SI sections 5.2.5, 5.3.5, 5.4.5 and 5.5.5).

The results of the exchange reactions demonstrate that not only the amidoboronate but also the iminoboronate influences the outcome of the exchange reaction with the amount of exchange typically increasing with more electron-rich amidoboronates and/or more electron-deficient iminoboronates. Exchange could be the result of several mechanisms such as a radical/dimer equilibrium from reversible C–C bond formation or oxidative C–C bond cleavage where any resulting radicals recombine or a two-electron reduced species reacts with an iminoboronate to form the cross-coupled dimer or homo-coupled dimer of the added iminoboronate (Fig. 3a). The possibility of a pathway to dimers *via* a two-electron reduced species is suggested by the loss of the cobaltocene addition product and corresponding appearance of cross-coupled amidoboronate dimers in exchange reactions (Fig. 3b).

We further investigated if the exchange reactions are based on a radical/dimer equilibrium or rather on redox reactions by performing control experiments where either equilibrated reaction mixtures or solutions of redissolved crystals were added together. If a radical/dimer equilibrium were present for the individual amidoboronate mixtures, the addition of a second set of amidoboronates should lead to cross-coupled amidoboronates species.

Thus, equilibrated mixtures of *p*-NMe_2 amidoboronates **5e** and **6e** were added to the corresponding mixtures of *p*-OMe amidoboronates **5d** and **6d**, respectively (Fig. S175 and S176). The isomeric ratios of the individual species did not change and there was no evidence of cross-coupled dimers in the ^{1}H NMR spectra. For the redissolved crystal experiments, amidoboronates **5c/d** were chosen to be added to **5e** since they reliably crystallize as the *rac* isomers only[24,25] and to probe a potential radical/dimer equilibrium for **5e**. Two sets of experiments were run for each amidoboronate pair where solutions of the redissolved crystals were: (i) immediately mixed; (ii) first equilibrated separately to allow for any *rac*$_5$–*rac*$_6$ interconversion[24,25] to occur before combining the solutions. Again, there was no indication that cross-coupled dimers formed upon mixing the crystals pre- (Fig. S177 and S179) or post-equilibration (Fig. S178 and S180). This implies that either a radical/dimer equilibrium is not present or alternatively, the reactivity and/or concentration of radicals is not sufficient to form cross-coupled species.

While these control experiments suggest exchange is less likely to occur *via* a radical/dimer equilibrium than a redox pathway, it cannot be completely excluded. Nevertheless, the observation of exchange demonstrates the dynamic covalent nature of the C–C bond, as evidenced by the formation of cross-coupled and new homo-coupled dimers as well as the disappearance of the cobaltocene addition product upon addition of a second iminoboronate.

Finally, the dynamic nature of the C–C bond was exploited in a diastereoselective transformation; we envisaged one diastereomer could be transformed into another using amidoboronates that result from a diastereoselective reductive coupling and undergo exchange readily (Fig. 5a). Thus, amidoboronates **7d** and **5e** were chosen since the reductive coupling led to *meso* and *rac* products, respectively (Fig. 1a and c). Therefore, the corresponding iminoboronates **1e** or **3d** were added to investigate if the transformation occurs *via* exchange (SI section 7).

Addition of two equivalents of **1e** (relative to the amidoboronate) to ***meso*$_5$-7d** led to minor spectral changes (Fig. S200); the original methine signals remained and there was no evidence of liberation of iminoboronate **3d**. However, the appearance of a small signal for ***rac*$_5$-5e** was consistent with the disappearance of the cobaltocene addition product of **7d**. Conversely, more significant spectral changes were observed upon addition of two equivalents of **3d** to ***rac*$_{5/6}$-5e** (Fig. S201); after one day, signals for **1e** and ***meso*$_5$-7d** appeared and increased over time, while those for ***rac*$_5$-5e** decreased relative to ***rac*$_6$-5e** until they almost completely disappeared after three days. Based on the integrals of ***meso*$_5$-7d** and ***rac*$_6$-5e**, a *rac* to *meso* conversion of 75% was estimated.

This experiment reveals the transformation from ***rac*-5e** to ***meso*$_5$-7d** is, in principle, possible and we then investigated whether an excess of **3d** could increase conversion to ***meso*$_5$-7d**. Indeed, upon addition of four equivalents of **3d** the highly diastereoselective transformation of ***rac*$_{5/6}$-5e** to ***meso*$_5$-7d** was observed (Fig. 5a and 6a–b); after four days, the mixture contained 92% ***meso*$_5$-7d** and 8% ***rac*$_6$-5e** along with trace amounts of other homo- and cross-coupled dimers (Fig. S202). Accurate quantification of the reaction mixture was not possible due to signal overlap of some homo- and cross-coupled dimer signals. Thus, it was possible to transform ***rac*$_5$-5e** to ***meso*$_5$-7d** but not *vice versa*, suggesting that dimer C–C bond can be broken upon addition of **3d** to **5e** but not **1e** to **7d**.

To gain insight into the diastereoselectivity of the transformation, two additional reductive couplings were carried out where iminoboronates **1e** and **3d** were present from the beginning in different ratios. For the first reaction, one equivalent each of the iminoboronates was reacted with two equivalents of cobaltocene to ensure there was enough reductant to consume all of the iminoboronate. From the maximum eight expected products (***meso*$_5$-7d**, ***rac*$_5$-7d**, ***rac*$_6$-7d**, ***rac*$_5$-5e**, ***rac*$_6$-5e** and the respective cross-coupled *meso*$_5$, *rac*$_5$ and *rac*$_6$ dimers), only six were observed with ***rac*$_5$-7d** and ***rac*$_6$-7d** likely not visible due to low signal intensity and/or overlap (Fig. S203).

In contrast, the second reductive coupling with a 4 : 2 : 2 **3d**/**1e**/Cp_2Co ratio (mimicking the exchange reaction with excess iminoboronate) gave ***meso*$_5$-7d** as the predominant product

Open Access Article. Published on 16 October 2025. Downloaded on 12/25/2025 7:24:13 PM.
This article is licensed under a Creative Commons Attribution 3.0 Unported Licence.

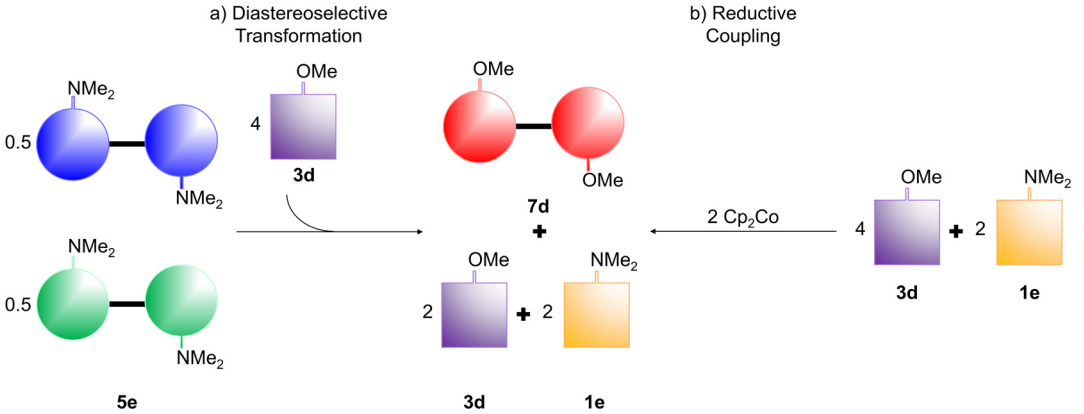

Fig. 5 (a) Diastereoselective transformation of a 1 : 1 ***rac*$_5$-5e** (blue) and ***rac*$_6$-5e** (green) mixture to ***meso*$_5$-7d** (red) upon addition of 4 eq. iminoboronate **3d** (purple); (b) reductive coupling of 4 eq. **3d** (purple) and 2 eq. **1e** (orange) resulting in the same products (***meso*$_5$-7d**, **3d**, **1e**).

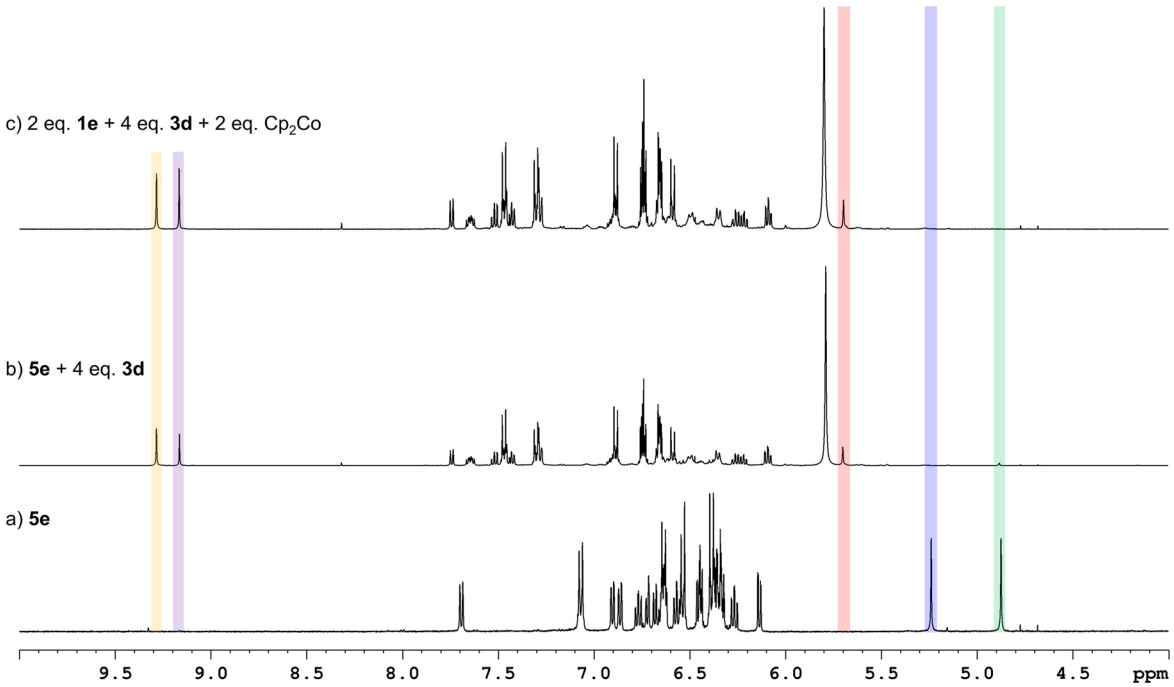

Fig. 6 NMR spectra (500 MHz, DMSO-d_6) of the diastereoselective transformation from (a) a 1 : 1 mixture of ***rac*$_5$-5e** (blue) and ***rac*$_6$-5e** (green) to (b) ***meso*$_5$-7d** (red); (c) diastereoselective reductive coupling of 2 eq. **1e** and 4 eq. **3d** with 2 eq. Cp_2Co. The unreacted/released imine signals of **1e** (purple) and **3d** (orange) are shown in each transformation.

with trace amounts of homo-coupled and cross-coupled dimers (Fig. 5b, 6c and S205). Quantification of the product distribution was difficult due to the signal overlap of some methine signals for the homo- and cross-coupled dimers. Nevertheless, the diastereoselectivity of this reductive coupling as well as the diastereoselective transformation from ***rac*$_{5/6}$-5e** to ***meso*$_5$-7d** suggest that ***meso*$_5$-7d** is the thermodynamic product and the system is under thermodynamic control since the same outcome is obtained independent of the reaction pathway. This could clarify why no exchange was observed upon addition of **1e** to ***meso*$_5$-7d**. Thus, the diastereoselectivity for ***meso*$_5$-7d** in both the transformation from ***rac*$_{5/6}$-5e** and the reductive coupling with 2 : 1 **3d**/**1e** is remarkable since, in theory, up to eight products could form.

Conclusion

The reductive coupling of *N*-aryl iminoboronates **1–4** gave up to three amidoboronate products (*rac*$_5$, *rac*$_6$ and *meso*$_5$) and in some reactions, another product proposed to be a cobaltocene addition product from two-electron reduction by cobaltocene.

This journal is © The Royal Society of Chemistry 2025

Open Access Article. Published on 16 October 2025. Downloaded on 12/25/2025 7:24:13 PM. This article is licensed under a Creative Commons Attribution 3.0 Unported Licence.

However, three reductive couplings were highly diastereoselective: **5e** for the *rac* isomer (as a 1 : 1 rac_5/rac_6 mixture); **7d** and **8d** for the $meso_5$ isomer (9 : 1 dr). Given the rarity of *meso* diastereoselective reductive couplings,[40–42] this importantly demonstrates that both diastereomers can be readily accessed through subtle modifications to the iminoboronate; a *p*-NMe_2 substituted aniline is proposed to favor the *rac* isomers, whereas a 3-fluoro-substituted phenylboronate typically favors the $meso_5$ isomer.

Reversible C–C bond formation was probed in exchange reactions by addition of a second iminoboronate, resulting in many cases in liberation of the original iminoboronate and formation of new homo- and/or cross-coupled amidoboronates. The degree of reversibility tended to increase with more electron-donating *p*-anilines and also depended on the added iminoboronate; little to no exchange was observed upon the addition of *p*-NMe_2 based iminoboronates (*e.g.* **1–4e**), while addition of **1–4a** (with *p*-Cl aniline) led to significant exchange.

Finally, the reversibility of C–C bond formation was exploited in the unprecedented diastereoselective transformation of ***rac*$_{5/6}$-5e** into predominantly ***meso*$_5$-7d** by addition of excess of **3d**. Conversely, the transformation of ***meso*$_5$-7d** into ***rac*-5e** was not observed. This transformation of a *rac* dimer into a different *meso* dimer with high diastereoselectivity is remarkable given, in principle, six products could be formed as a mixture of homo- and cross-coupled dimers based on a control reductive coupling with both iminoboronates present.

Thus, this work demonstrates proof-of-principle for the application of the reductive coupling in the self-assembly of amidoboronate-based macrocycles and cages since the diastereoselectivity and the reversibility of C–C bond formation can be controlled through the judicious choice of the *p*-aniline, catechol and phenylboronate substituents. Furthermore, it opens up new opportunities for not only controlling diastereoselectivity but also constructing more complex dynamic covalent systems; taking advantage of the dynamic covalent B–N,[24,25] B–O[25] and C–C bonds of amidoboronates, future work will investigate the orthogonality of these three dynamic covalent bonds in stereoselective transformations.

Author contributions

PH: conceptualization, data curation, formal analysis, investigation, resources, validation, visualisation, writing – original draft, writing – review and editing. TR: data curation, formal analysis, software, visualisation, writing – review and editing. LP: formal analysis, investigation, resources, writing – review and editing. CN: formal analysis, investigation, resources, writing – review and editing. BH: resources, supervision, writing – review and editing. AJM: conceptualisation, formal analysis, funding acquisition, project administration, supervision, visualisation, writing – original draft, writing – review and editing.

Conflicts of interest

There are no conflicts to declare.

Data availability

Data for this article, including characterisation and computational are available at FoDaSi at https://doi.org/10.25819/jn42pe309915uugx.

The data supporting this article have been included as part of the supplementary information (SI). Supplementary information: additional references.[10,19–21,23–25,52,53,55,62–74] See DOI: https://doi.org/10.1039/d5ob01479d.

CCDC 2415221 (**8d**), 2415535 (**3a**) and 2415536 (**4d**) contain the supplementary crystallographic data for this paper.[75a–c]

Acknowledgements

We thank the Deutsche Forschungsgemeinschaft (DFG, project number 447862786) for financial support and Thomas Brandt, Anton Kaus, Anke Sehrer and Michaela Taddey for preliminary studies. We thank the spectroscopy department for NMR and mass spectral data collection.

References

1 S. J. Rowan, S. J. Cantrill, G. R. L. Cousins, J. K. M. Sanders and J. F. Stoddart, *Angew. Chem., Int. Ed.*, 2002, **41**, 898–952.
2 R.-C. Brachvogel and M. von Delius, *Eur. J. Org. Chem.*, 2016, 3662–3670.
3 A.-E. Dascalu, L. Halgreen, A. Torres-Huerta and H. Valkenier, *Chem. Commun.*, 2022, **58**, 11103–11106.
4 D. Sakamaki, S. Ghosh and S. Seki, *Mater. Chem. Front.*, 2019, **3**, 2270–2282.
5 A. Wilson, G. Gasparini and S. Matile, *Chem. Soc. Rev.*, 2014, **43**, 1948–1962.
6 J.-M. Lehn, *Chem. Soc. Rev.*, 2007, **36**, 151–160.
7 F. Beuerle and B. Gole, *Angew. Chem., Int. Ed.*, 2018, **57**, 4850–4878.
8 A. Stoy, M. Jürgensen, C. Millidoni, C. Berthold, J. Ramler, S. Martínez, M. R. Buchner and C. Lichtenberg, *Angew. Chem., Int. Ed.*, 2023, **62**, e202308293.
9 D. Hartmann and L. Greb, *Angew. Chem., Int. Ed.*, 2020, **59**, 22510–22513.
10 T. Kobashi, D. Sakamaki and S. Seki, *Angew. Chem., Int. Ed.*, 2016, **55**, 8634–8638.
11 D. Beaudoin, O. Levasseur-Grenon, T. Maris and J. D. Wuest, *Angew. Chem., Int. Ed.*, 2016, **55**, 894–898.
12 Y. Liu, H. Yi, T. Tao, P. Hoa and C. Chunyan, *Angew. Chem., Int. Ed.*, 2018, **57**, 9023–9027.
13 K. Oda, S. Hiroto and H. Shinokubo, *J. Mater. Chem. C*, 2017, **5**, 5310–5315.

Open Access Article. Published on 16 October 2025. Downloaded on 12/25/2025 7:24:13 PM. This article is licensed under a Creative Commons Attribution 3.0 Unported Licence.

14 P. H. Kirchner, L. Schramm, S. Ivanova, K. Shoyama, F. Würthner and F. Beuerle, *J. Am. Chem. Soc.*, 2024, **146**, 5305–5315.
15 X. Wang, O. Shyshov, M. Hanževački, C. M. Jäger and M. von Delius, *J. Am. Chem. Soc.*, 2019, **141**, 8868–8876.
16 M. M. Perera and N. Ayres, *Polym. Chem.*, 2020, **11**, 1410–1423.
17 Z. Ma, S. Pan, Y. Yang, Y. Zeng, B. Wang, Y. Wei and L. Tao, *Nat. Commun.*, 2025, **16**, 3679.
18 S. Delpierre, B. Willocq, G. Manini, V. Lemaur, J. Goole, P. Gerbaux, J. Cornil, P. Dubois and J.-M. Raquez, *Chem. Mater.*, 2019, **31**, 3736–3744.
19 K. Okino, S. Hira, Y. Inoue, D. Sakamaki and S. Seki, *Angew. Chem., Int. Ed.*, 2017, **56**, 16597–16601.
20 R. Zhang, J. P. Peterson, L. J. Fischer, A. Ellern and A. H. Winter, *J. Am. Chem. Soc.*, 2018, **140**, 14308–14313.
21 J. P. Peterson, M. R. Geraskina, R. Zhang and A. H. Winter, *J. Org. Chem.*, 2017, **82**, 6497–6501.
22 J. P. Peterson and A. H. Winter, *J. Am. Chem. Soc.*, 2019, **141**, 12901–12906.
23 R. Zhang, A. Ellern and A. H. Winter, *J. Org. Chem.*, 2022, **87**, 1507–1511.
24 E. N. Keyzer, A. Sava, T. K. Ronson, J. R. Nitschke and A. J. McConnell, *Chem. – Eur. J.*, 2018, **24**, 12000–12005.
25 P. Harders, T. Griebenow, A. Businski, A. J. Kaus, L. Pietsch, C. Näther and A. J. McConnell, *ChemPlusChem*, 2022, **87**, e202200022.
26 A. J. McConnell, *Dalton Trans.*, 2023, **52**, 9189–9201.
27 R. Fittig, *Justus Liebigs Annalen der Chemie*, 1859, **110**, 23–45.
28 J. E. McMurry and R. G. Dushin, *J. Am. Chem. Soc.*, 1989, **111**, 8928–8929.
29 T. Mukaiyama, T. Sato and J. Hanna, *Chem. Lett.*, 2006, **2**, 1041–1044.
30 A. Chatterjee and N. N. Joshi, *Tetrahedron*, 2006, **62**, 12137–12158.
31 M. Jung and U. Groth, *Synlett*, 2002, 2015–2018.
32 T. Mukaiyama, N. Yoshimura, K. Igarashi and A. Kagayama, *Tetrahedron*, 2001, **57**, 2499–2506.
33 J. Sun, Z. Dai, C. Li, X. Pan and C. Zhu, *J. Organomet. Chem.*, 2009, **694**, 3219–3221.
34 H. Yang, H. Wang and C. Zhu, *J. Org. Chem.*, 2007, **72**, 10029–10034.
35 Y.-G. Li, Q.-S. Tian, J. Zhao, Y. Feng, M.-J. Li and T.-P. You, *Tetrahedron: Asymmetry*, 2004, **15**, 1707–1710.
36 F. Calogero, G. Magagnano, S. Potenti, F. Pasca, A. Fermi, A. Gualandi, P. Ceroni, G. Bergamini and P. G. Cozzi, *Chem. Sci.*, 2022, **13**, 5973–5981.
37 A. Chatterjee, T. H. Bennur and N. N. Joshi, *J. Org. Chem.*, 2003, **68**, 5668–5671.
38 J. G. Smith and C. D. Veach, *Can. J. Chem.*, 1966, **44**, 2497–2502.
39 J. G. Smith and I. Ho, *J. Org. Chem.*, 1972, **37**, 653–656.
40 Y. Mitoma, I. Hashimoto, C. Simion, M. Tashiro and N. Egashira, *Synth. Commun.*, 2008, **38**, 3243–3250.
41 H. C. Aspinall, N. Greeves and C. Valla, *Org. Lett.*, 2005, **7**, 1919–1922.
42 B. Hatano, A. Ogawa and T. Hirao, *J. Org. Chem.*, 1998, **63**, 9421–9424.
43 Z. X. Giustra and S.-Y. Liu, *J. Am. Chem. Soc.*, 2018, **140**, 1184–1194.
44 C. R. McConnell and S.-Y. Liu, *Chem. Soc. Rev.*, 2019, **48**, 3436–3453.
45 M. Hejda, R. Jambor, A. Růžička, A. Lyčka and L. Dostál, *Dalton Trans.*, 2014, **43**, 9012–9015.
46 M. Yamashita, Y. Aramaki and K. Nozaki, *New J. Chem.*, 2010, **34**, 1774–1782.
47 J. N. Dahanayake, C. Kasireddy, J. P. Karnes, R. Verma, R. M. Steinert, D. Hildebrandt, O. A. Hull, J. M. Ellis and K. R. Mitchell-Koch, in *Annual Reports on NMR Spectroscopy*, ed. G. A. Webb, Academic Press, 2018, vol. 93, pp. 281–365.
48 W. Ni, G. Kaur, G. Springsteen, B. Wang and S. Franzen, *Bioorg. Chem.*, 2004, **32**, 571–581.
49 X. Sun, T. D. James and E. V. Anslyn, *J. Am. Chem. Soc.*, 2018, **140**, 2348–2354.
50 L. Zhu, S. H. Shabbir, M. Gray, V. M. Lynch, S. Sorey and E. V. Anslyn, *J. Am. Chem. Soc.*, 2006, **128**, 1222–1232.
51 X. Sun, B. M. Chapin, P. Metola, B. Collins, B. Wang, T. D. James and E. V. Anslyn, *Nat. Chem.*, 2019, **11**, 768–778.
52 M. Ishimoto, D. Sakamaki and H. Fujiwara, *Chem. Commun.*, 2022, **58**, 3553–3556.
53 H. Hasegawa, D. Sakamaki and H. Fujiwara, *Angew. Chem., Int. Ed.*, 2023, **62**, e202302498.
54 H. G. Viehe, Z. Janousek, R. Merenyi and L. Stella, *Acc. Chem. Res.*, 1985, **18**, 148–154.
55 E. Blokker, M. ten Brink, J. M. van der Schuur, T. A. Hamlin and F. M. Bickelhaupt, *ChemistryEurope*, 2023, e202300006.
56 E. O. Fischer and G. E. Herberich, *Chem. Ber.*, 1961, **94**, 1517–1523.
57 M. L. H. Green, L. Pratt and G. Wilkinson, *J. Chem. Soc.*, 1959, 3753–3767.
58 G. E. Herberich, E. Bauer and J. Schwarzer, *J. Organomet. Chem.*, 1969, **17**, 445–452.
59 G. E. Herberich and J. Schwarzer, *Angew. Chem., Int. Ed. Engl.*, 1970, **9**, 897–897.
60 M. Enders, G. Kohl and H. Pritzkow, *Organometallics*, 2004, **23**, 3832–3839.
61 H. P. Fritz and H. J. Keller, *Chem. Ber.*, 1962, **95**, 2259–2263.
62 G. Sheldrick, *Acta Crystallogr., Sect. A: Found. Adv.*, 2015, **71**, 3–8.
63 G. Sheldrick, *Acta Crystallogr., Sect. C: Struct. Chem.*, 2015, **71**, 3–8.
64 P. J. Stephens, F. J. Devlin, C. F. Chabalowski and M. J. Frisch, *J. Phys. Chem.*, 1994, **98**, 11623–11627.
65 F. Weigend and R. Ahlrichs, *Phys. Chem. Chem. Phys.*, 2005, **7**, 3297–3305.
66 F. Weigend, *Phys. Chem. Chem. Phys.*, 2006, **8**, 1057–1065.

 This journal is © The Royal Society of Chemistry 2025

Open Access Article. Published on 16 October 2025. Downloaded on 12/25/2025 7:24:13 PM.
This article is licensed under a Creative Commons Attribution 3.0 Unported Licence.

67 F. Neese, *Wiley Interdiscip. Rev.: Comput. Mol. Sci.*, 2022, **12**, e1606.
68 F. Neese, F. Wennmohs, U. Becker and C. Riplinger, *J. Chem. Phys.*, 2020, **152**, 224108.
69 F. Neese, *J. Chem. Theory Comput.*, 2023, **44**, 381–396.
70 E. Caldeweyher, S. Ehlert, A. Hansen, H. Neugebauer, S. Spicher, C. Bannwarth and S. Grimme, *J. Chem. Phys.*, 2019, **150**, 154122.
71 F. Neese, *J. Chem. Theory Comput.*, 2003, **24**, 1740–1747.
72 F. Neese, F. Wennmohs, A. Hansen and U. Becker, *Chem. Phys.*, 2009, **356**, 98–109.
73 C. Bannwarth, S. Ehlert and S. Grimme, *J. Chem. Theory Comput.*, 2019, **15**, 1652–1671.
74 S. Saha, R. K. Roy and P. W. Ayers, *Int. J. Quantum Chem.*, 2009, **109**, 1790–1806.
75 (*a*) CCDC 2415221: Experimental Crystal Structure Determination, 2025, DOI: 10.5517/ccdc.csd.cc2m27cb; (*b*) CCDC 2415535: Experimental Crystal Structure Determination, 2025, DOI: 10.5517/ccdc.csd.cc2m2khs; (*c*) CCDC 2415536: Experimental Crystal Structure Determination, 2025, DOI: 10.5517/ccdc.csd.cc2m2kjt.